JOURNAL OF MATERIALS SCIENCE 8 (1973) 928–940

Anisotropy of the mechanical α-relaxation in biaxially oriented linear polyethylene

C. P. BUCKLEY,* N. G. McCRUM
Department of Engineering Science, University of Oxford, Oxford, UK

Alternative theories for the origin of the high temperature, α-relaxation in oriented linear polyethylene are compared with experiment. The α-mechanism is assumed to be simple shear by all theories which differ in the allocation of the shear plane. The theories take the shear plane to be the interlamellar surface (theory I), a crystal plane of type (*hk*0) (theory IIA), a crystal plane of type (*h*00) (theory IIB). The experiments comprise measurements of the creep tensile compliance $D(t)$ on oriented specimens at angles 0°, 45° and 90° to the draw axis. The crucial test involves the examination of specimens with approximately the same crystallographic orientation (determined by wide-angle X-ray diffraction) but differing orientation of lamellar normals. The analysis is based on the Reuss, constant stress hypothesis. It is shown that with this assumption, only theory I agrees with experiment.

1. Introduction

Linear polyethylene (LPE) typically exhibits two mechanical relaxations between room temperature and the melting point, for measuring frequencies of about 1 Hz. They are labelled α and α' in order of increasing temperature at which they occur. The mechanisms so far suggested for mechanical relaxation in this temperature range in LPE, largely fall into the following three groups.

I. Interlamellar shear: mechanical relaxation occurs in response to shear stresses acting in the plane of the non-crystalline layer separating adjacent lamellar crystals [1-6].

II. Intracrystalline shear: mechanical relaxation occurs within the crystals, by relative displacement of molecules parallel to the chain axis [7-9]. Relaxation will be manifest for shear stresses within the crystal of type ($hk0$) [00l], with either (A) h and k arbitrary integers, or (B) $k = 0$ if relaxation is confined to shear on (h00) planes as suggested by some authors [7, 9].

III. Incoherent lattice vibration: mechanical relaxation occurs within the crystals because of viscous interaction between molecules, caused by the onset of incoherent lattice vibrations [10-13].

Of these three suggestions, both I and II assign mechanical relaxation to a deformation process of simple shear. They predict a highly anisotropic relaxation magnitude for samples with preferred orientation of either lamellar surfaces (theory I) or crystal axes (theory II). Clearly, this suggests an attractive experimental method of choosing at least between theories I and II. As yet, however, there has been no attempt to observe the effect on relaxation magnitude in LPE of varying, independently, the orientation of lamellar surfaces and crystal axes.

The present study was designed to carefully test theories I, IIA and IIB, by bringing together two recent developments in polymer science. These are, firstly, the availability of specimens of LPE with high and unambiguous lamellar [14] and crystallographic [15] orientation, and secondly the application of computer controlled X-ray diffractometers for measuring complete crystal orientation in oriented polymers. This enabled specimens to be prepared with nearly unique orientation of each of vectors **a**, **b**, **c** and $\mathbf{n}_1$ (unit normal to the lamella surface). Furthermore, in order to make possible a choice between theories I and II, specimens were prepared with similar crystal orientation but differing lamellar orientation.

The special orientation procedure used in this work consisted of drawing under conditions of essentially pure shear. That is to say, drawing was accompanied by simultaneous lateral constraint

*Present address: Centre de Recherches sur les Macromolécules, 6 Rue Boussingault, 67-Strasbourg, France.

© *1973 Chapman and Hall Ltd.*

in the plane of the sheet, a method previously adopted by Seto and Hara [14]. This produced highly-oriented sheets containing biaxial orientation. Lamellar orientation was controlled by simply varying the temperature of drawing. Here we report tensile creep measurements in the α-relaxation region of temperature, made on just two such drawn sheets containing widely differing lamellar orientations.

2. Experimental

2.1. Biaxially cold-drawn LPE

The initial material for preparation of all samples of oriented LPE was 3 mm thick plate of Rigidex 2*, compression moulded at 155°C and quenched from the melt into water at room temperature. The resulting density at 23°C was $\rho(23) = 0.950$ g cm^{-3}.

The sheet of biaxially cold-drawn LPE studied here has been described before [15], but important details will be given again. It was prepared by drawing such a plate to a draw ratio of 7 at room temperature, while maintaining the plate width nearly constant. This was achieved by starting with an initial length to width ratio of only 1:9, thereby causing the clamps to exert lateral constraint on the sheet during neck formation. After annealing without constraint at 127°C for 1 h the resulting sheet was transparent and of density $\rho(23) = 0.967$ g cm^{-3}.

Orientations of each of crystal axes *a*, *b* and *c* were measured directly by means of wide-angle X-ray pole figures for (200), (020) and (002) poles, obtained following the procedure outlined before [15]. Pole figures are presented here as polar plots in terms of polar angles ψ and χ, defined with respect to reference directions *X*, *Y* and *Z* in the oriented sheet in Fig. 1. Pole figures for (200), (020) and (002) poles are shown in Fig. 2a, b and c respectively. Because of the high orientation of *c*-axes, the whole scattering hemisphere is not shown. Instead, a range of just 30° in χ is covered. Thus Fig. 2a and b cover the range $0° < \psi < 360°$, $60° < \chi < 90°$ while Fig. 2c covers the range $0° < \psi < 360°$ $0° < \chi < 30°$. Contours shown occur at intervals of 10% of maximum intensity. Fig. 2a shows *a*-axes to have preferred orientation in the *XZ* plane at ±5° to *X*. Fig. 2b shows *b*-axes to have a single preferred orientation parallel to *Y*. Accordingly, *c*-axes are shown by Fig. 2c to lie preferentially in the *XZ* plane at ±5° to *Z*.

The same oriented sheet was studied by small-angle X-ray scattering. Patterns obtained with the beam in *X* and *Y* directions are shown in Fig. 3a and b respectively. In each case, specimen thickness and photograph preparation conditions were identical, so that the intensities of the two patterns may be compared. It is clear from the intense four-point pattern of Fig. 3b that lamella normals $\mathbf{n}_1$ lie preferentially in the *XZ* plane at ±38° to *Z*.

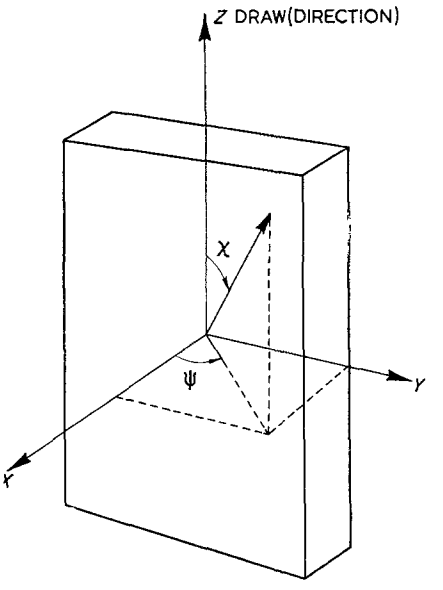

Figure 1 Definition of axes and co-ordinates in oriented polyethylene sheet.

The above X-ray evidence may be summarized by the idealized doublet structural model shown in Fig. 4a. Crystalline and non-crystalline regions are stacked in regular layers, with *a*- and *c*-axes and lamella normals $\mathbf{n}_1$ in the directions indicated. Crystal *b*-axes lie parallel to *Y*.

2.2. Biaxially hot-drawn LPE

The initial material was again a quenched compression-moulded plate of Rigidex 2. This plate was drawn in air at 121°C in a box immersed in a silicone oil-bath. The sheet width was again maintained nearly constant during drawing, and a uniform draw ratio of 9 was achieved within the necked region. The resulting transparent sheet was then annealed without constraint at 127°C for 1 h, after which it was still transparent and of density $\rho(23) = 0.971$ g cm^{-3}. Throughout the drawing and annealing sequence care was taken to reproduce as closely

*BP Chemicals Ltd.

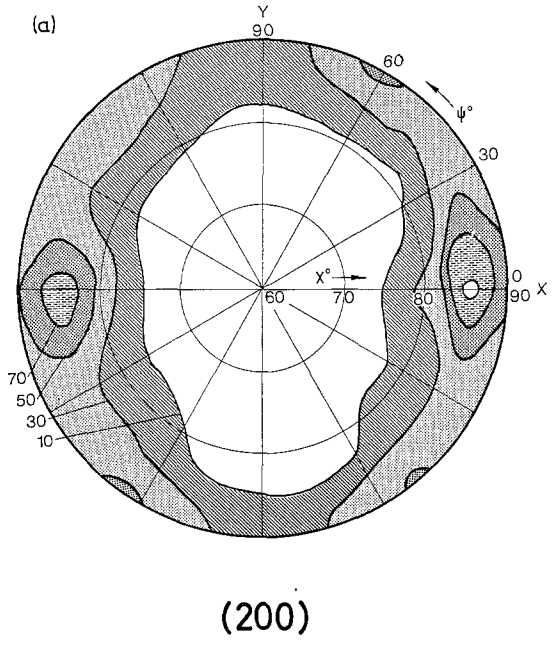

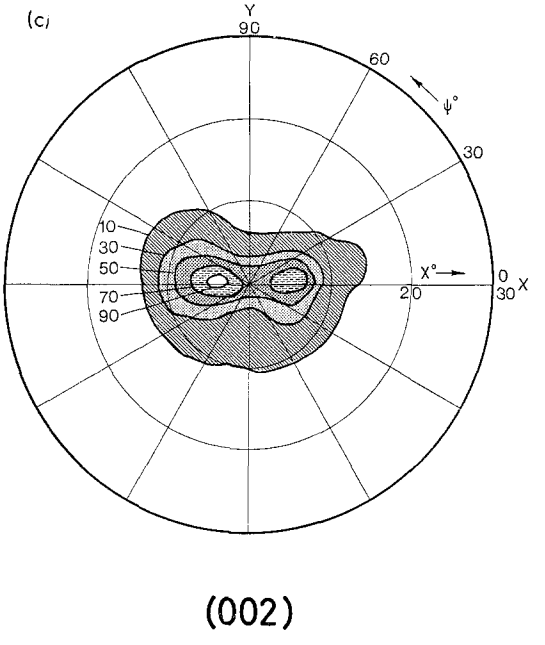

Figure 2 Wide-angle X-ray pole figures for biaxially cold-drawn LPE: (a) (200) pole figure, (b) (020) pole figure, (c) (002) pole figure.

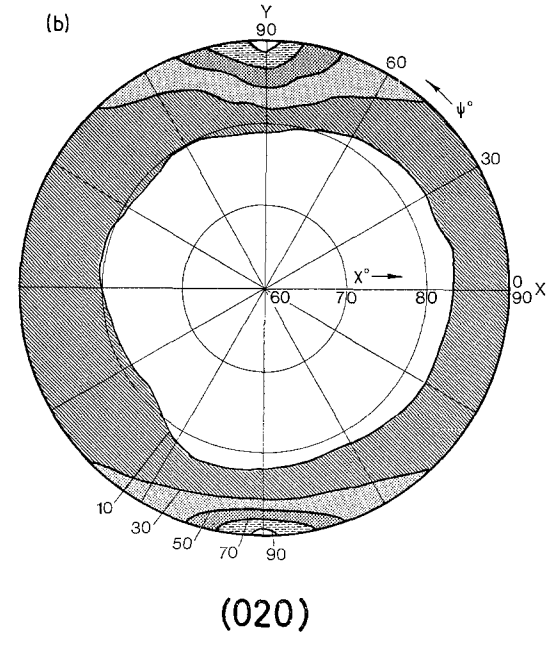

as possible, in all details except draw temperature, the method of preparation of the biaxially cold-drawn sheet.

Wide-angle X-ray pole figures obtained for (200), (020) and (002) poles are shown in Fig. 5a, b and c respectively. Again, only a portion of the scattering hemisphere is covered. Fig. 5a and b covers the range $0° < \psi < 360°$, $60° < \chi < 90°$ and contours occur at intervals of 10% of maximum intensity. Fig. 5c covers the range $0° < \psi < 360°$, $0° < \chi < 30°$, and, for the sake of clarity, only 10, 30, 50, 70 and 90% contours are shown. Fig. 5a, b and c show *a*-, *b*-, and *c*-axes to have single preferred orientations parallel to *X*, *Y* and *Z* respectively. Small-angle X-ray scattering patterns obtained from this sheet are shown in Fig. 6a and b for the beam in

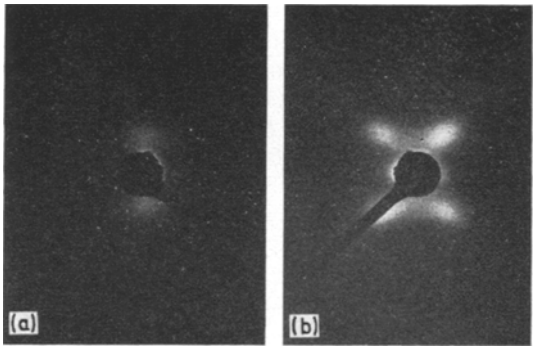

Figure 3 Small-angle X-ray diffraction patterns from biaxially cold-drawn LPE (draw direction vertical): (a) beam parallel to *X*, (b) beam parallel to *Y*.

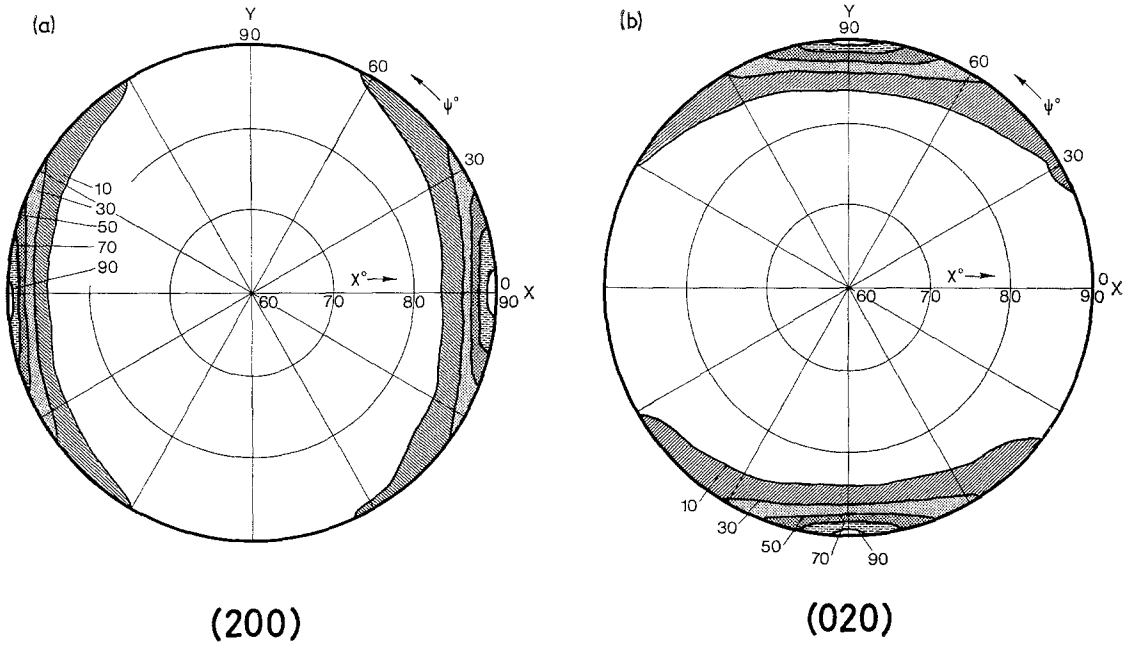

X and Y directions. The two-point patterns show $\mathbf{n}_1$ to lie preferentially parallel to Z, with probably a greater spread of orientations in the XZ plane than in the YZ plane, judging from the relative widths of the patterns.

Again, the X-ray evidence may be summarized by means of an idealized structural model. This is shown in Fig. 4b. It is clear that the special significance of this biaxially hot-drawn sheet of LPE is the unique preferred orientation of each of vectors **a**, **b**, **c** and $\mathbf{n}_1$. This type of orientation has never previously been reported for bulk samples of melt-crystallized LPE, although a similar result was obtained by drawing single crystal mats of LPE at 90°C [16].*

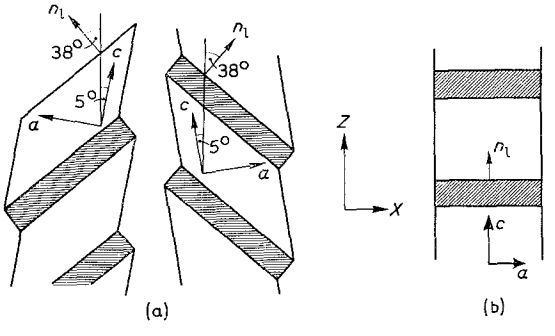

Figure 4 Idealized structural model of (a) biaxially cold-drawn LPE and (b) biaxially hot-drawn LPE.

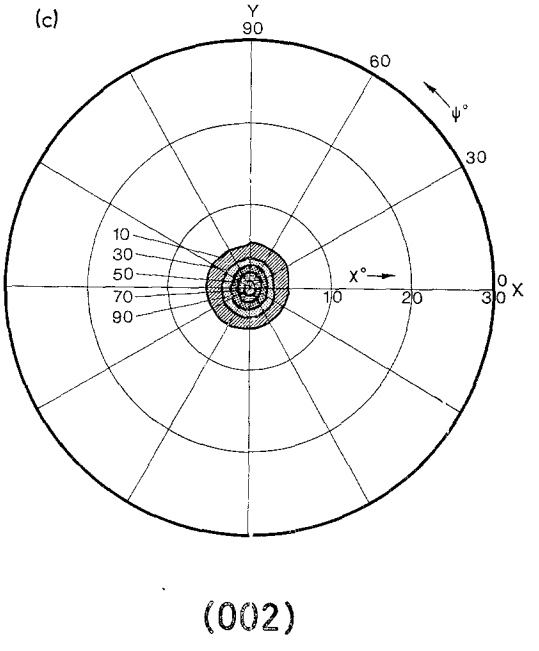

Figure 5 Wide-angle X-ray pole figures for biaxially hot-drawn LPE: (a) (200) pole figure, (b) (020) pole figure, (c) (002) pole figure.

*Samples of LPE with unique preferred orientation of each of vectors **a**, **b**, **c**, and $\mathbf{n}_1$ have recently been obtained using a different technique by R. J. Young *et al* (*J. Mater. Sci.* **8** (1973) 23).

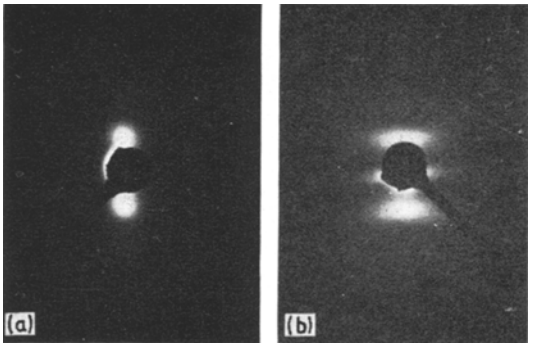

Figure 6 Small-angle X-ray diffraction patterns from biaxially hot-drawn LPE (draw direction vertical): (a) beam parallel to X, (b) beam parallel to Y.

2.3. Tensile creep measurements

From both oriented sheets described above tensile specimens were cut with tensile axes at various angles θ to Z. These were rectangular specimens of dimensions in the test section of 0.1 cm × 0.3 cm × 3.5 cm. Short term tensile creep tests were performed in the temperature range −80 to +80°C, using a tensile creep apparatus based on the principle of precision measurement of clamp displacement. This apparatus will be described elsewhere. The tensile creep compliance at temperature T, and creep time t, $D^T(t)$, was subject to error limits of ±5%, arising chiefly from measurement of specimen dimensions and irreproducibility of clamping the specimen. Scatter of points on a given creep curve, however, was always less than 0.5%. In order to maintain this precision, creep was terminated after 60 sec (below room temperature) or 180 sec (above room temperature), after which time a gradual shift of the baseline, owing to differential thermal expansion of different parts of the creep apparatus, caused a systematic error greater than 0.5%. During all creep tests, specimen temperature was maintained constant to within ±0.1°C.

The time/temperature sequence employed always consisted of changing temperature down (below room temperature) or up (above room temperature) in steps of between 5 and 10°C, allowing about 40 min for the system to equilibrate at each new temperature before performing the creep test. After each test a recovery time sufficient for complete recovery of the specimen (to within the sensitivity of measurement) was allowed before again changing temperature. In addition, care was always taken when cooling to cool at a rate of less than about 0.5°C min^{-1}, since rapid cooling of LPE, even below room temperature, gives rise to misleading mechanical properties [17].

All creep tests were conducted at tensile strains of less than 0.001. In this region of strain, no non-linearity in the viscoelastic behaviour of those samples of LPE studied here could usually be detected (the departures from linearity which were observed, even at such low strains, will be mentioned below). In the present study, creep curves were used to calculate tan $\delta^T(\omega)$, for a radial frequency ω, using the approximation method of Zener [18],

$$\tan \delta^T(\omega) \simeq \frac{\pi}{2}\left[\frac{\partial \ln D^T(t)}{\partial \ln t}\right]_{\omega=1/t} . \quad (1)$$

Equation 1 is a good approximation if the square bracket is small compared with unity and varies only slowly with ln t [18], conditions which prevailed here.

3. Results

In treating the anisotropy of $D^T(t)$ for samples of oriented LPE, we note that this material (at the low strains used here) is an anisotropic linear viscoelastic solid. To describe the anisotropy at constant T and t, we may, therefore, employ the formalism of anisotropic elasticity theory [19]. Stress and strain are then related by the matrix equation

$$\boldsymbol{\varepsilon} = \mathbf{S}\boldsymbol{\sigma} \quad (2)$$

where $\boldsymbol{\varepsilon}$ and $\boldsymbol{\sigma}$ are the 6-component column matrices of strain and stress and $\mathbf{S}$ the compliance matrix [20]. Those samples of LPE studied here have orthorhombic symmetry with principal axes X, Y, Z, as a consequence of the method of drawing. The matrix $\mathbf{S}$ therefore takes the form [20]

$$\mathbf{S} = \begin{bmatrix} S_{11} & S_{12} & S_{13} & 0 & 0 & 0 \\ S_{12} & S_{22} & S_{23} & 0 & 0 & 0 \\ S_{13} & S_{23} & S_{33} & 0 & 0 & 0 \\ 0 & 0 & 0 & S_{44} & 0 & 0 \\ 0 & 0 & 0 & 0 & S_{55} & 0 \\ 0 & 0 & 0 & 0 & 0 & S_{66} \end{bmatrix} \quad (3)$$

where subscripts 1, 2, 3 refer to axes X, Y, Z. For a tensile test with tensile axis in the YZ plane at an angle $\theta°$ to Z, the measured tensile compliance D_θ may be shown to be given by [20]

$$D_\theta = S_{22}\sin^4\theta + (2S_{23} + S_{44})\sin^2\theta\cos^2\theta + S_{33}\cos^4\theta . \quad (4)$$

Equation 4 applies equally to tensile creep compliance $D_\theta(t)$ or complex tensile compliance $D^*_\theta(\omega)$, if the matrix S corresponds to S(t) or S*(ω) respectively [19].

It is clear from Equation 4 that measurements of $D^T_\theta(t)$ at only three different values of θ are necessary to completely specify the angular dependence of D_θ in the YZ plane. Results are, therefore, presented here in terms of D_0, D_{45} and D_{90}, given by Equation 4 as

$$\left.\begin{aligned} D_0 &= S_{33} \\ D_{45} &= \tfrac{1}{4}(S_{22} + 2S_{23} + S_{44} + S_{33}) \\ D_{90} &= S_{22} \ . \end{aligned}\right\} \qquad (5)$$

Data from a creep curve $D^T_\theta(t)$ are represented by isochronal quantities D^T_θ(10 sec) and tan δ_θ(0.1 rad sec^{-1}) (obtained from Equation 1). The temperature dependence of these, at $\theta = 0°$, 45° and 90°, are shown in Figs. 7 and 8 for biaxially cold-drawn LPE and in Figs. 9 and 10 for biaxially hot-drawn LPE.

It has been shown before [21] that properly stabilized specimens of biaxially drawn LPE show only one relaxation in the temperature range considered here. We label this the "α-relaxation" but, without meaning at this stage to imply its identity to the α-relaxation observed in undrawn LPE (see below). Figs. 8 and 10 show the anisotropy of the α-relaxation, as expressed by tan δ, to take the form tan $\delta_0 >$ tan $\delta_{45} >$ tan δ_{90} for both cold-drawn and hot-drawn LPE.

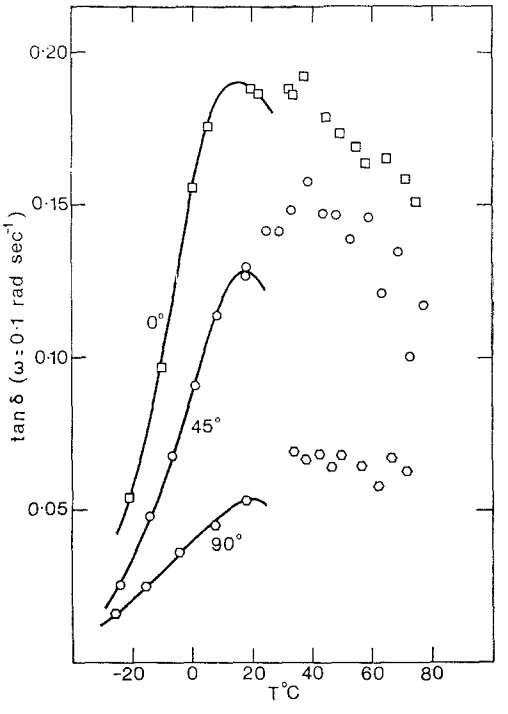

Figure 8 Biaxially cold-drawn LPE: tan δ derived from tensile creep curves, for $\theta = 0°$, 45° and 90°.

This is confirmed by the relative gradients of the $\log_{10} D_\theta{}^T$(10 sec) versus T plots of Figs. 7 and 9. Such a result is in agreement with all previous measures of the anisotropy of this relaxation in drawn and annealed LPE [5, 22, 23].

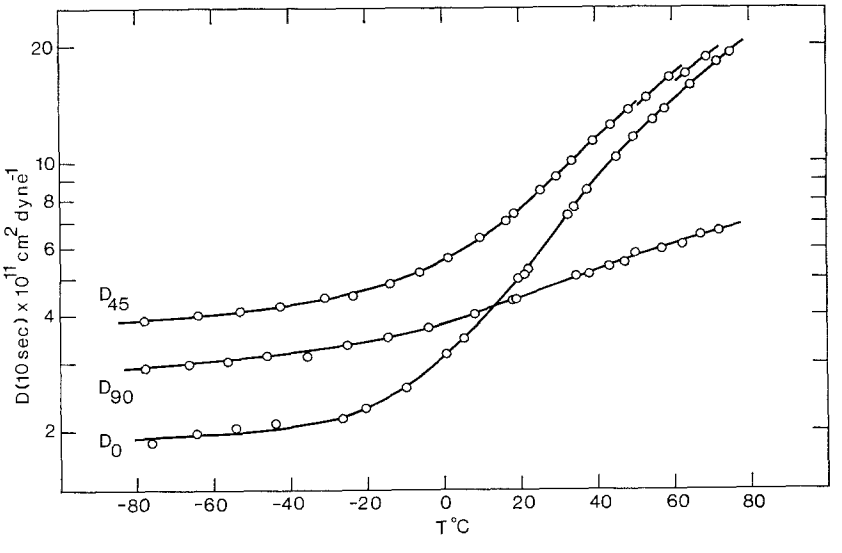

Figure 7 Biaxially cold-drawn LPE: tensile creep compliance $D_\theta{}^T$ (10 sec) plotted logarithmically versus temperature T, for $\theta = 0°$, 45° and 90°.

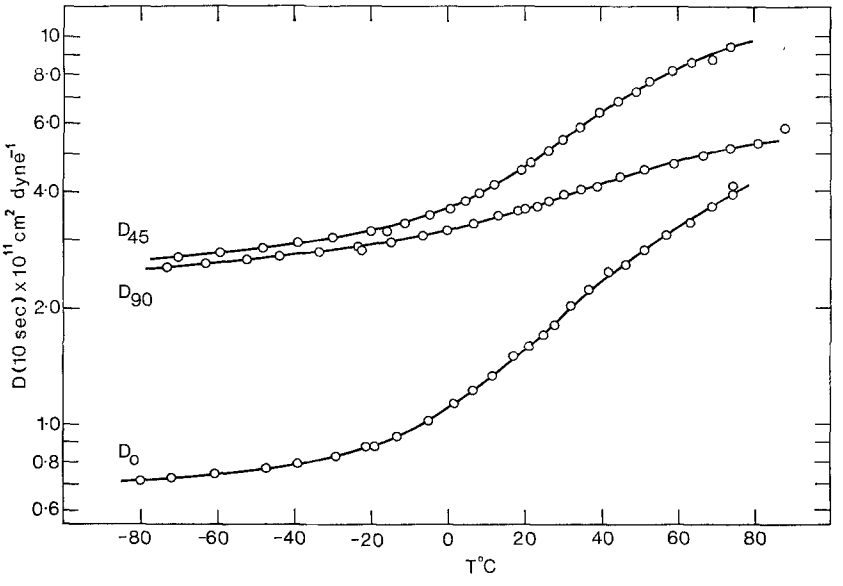

Figure 9 Biaxially hot-drawn LPE: tensile creep compliance $D_\theta{}^T$ (10 sec) plotted logarithmically versus temperature T, for $\theta = 0°$, 45° and 90°.

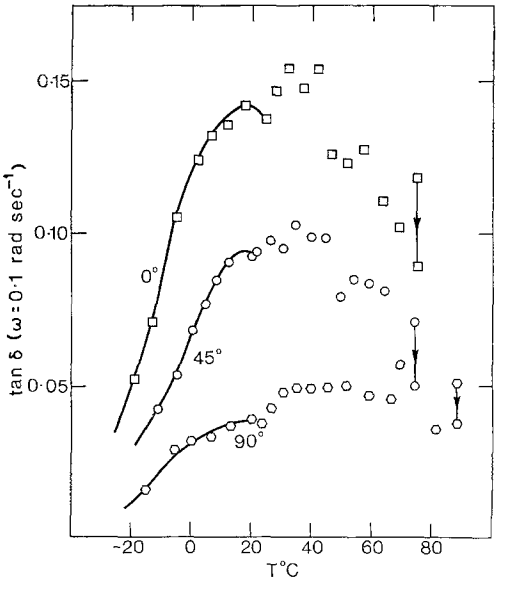

Figure 10 Biaxially hot-drawn LPE: tan δ derived from tensile creep curves, for $\theta = 0°$, 45° and 90°.

An interesting feature to emerge from the present work is the large difference between D_0 for biaxially hot-drawn LPE and D_0 for biaxially cold-drawn LPE (compare Figs. 7 and 9). In particular, the crossover between D_0 and D_{90}, which is usually observed in this temperature range for annealed cold-drawn LPE [22, 24] (see also Fig. 7), is absent in Fig. 9 for hot-drawn LPE. This arises mainly because of the low value of the unrelaxed D_0 in the latter case. The low temperature mechanical anisotropy of these samples will be discussed elsewhere.

The reader will note that above room temperature there is a high degree of scatter in tan δ, for all specimens studied here. This is a consequence of annealing effects occurring during the experiment, as shown in Fig. 10 where arrows indicate the effect on tan δ of maintaining constant temperature for 1 h. In spite of large changes in the gradients of creep curves (and hence tan δ) with time, however, the corresponding decrease in isochronal compliance D^T(10 sec) is barely discernible in Figs. 7 and 9. Since it is clear that in each case the specimen was changing during the course of the experiment above room temperature, all discussion below is based on results obtained at, or below, room temperature. The α-peak in tan δ can be easily resolved at such low temperatures at the low effective frequency employed here ($\omega = 0.1$ rad sec^{-1}). It should be remembered that these specimens had previously been carefully stabilized at 127°C, so the fact that annealing effects commence so soon above room temperature is particularly surprising. This phenomenon may, however, be related to the fact that the onset of partial melting in drawn LPE, even after extensive annealing at 127.5°C, occurs at unusually low temperatures [25].

Another disturbing effect on the data presented

here is the non-linear viscoelastic behaviour observed at high temperatures in some samples. This effect was only discernible in $D_{45}{}^{T}(10\ \text{sec})$ for biaxially cold-drawn LPE and at temperatures T greater than about 40°C. In Fig. 7, therefore, a solid curve is drawn through measures of $D_{45}{}^{T}(10\ \text{sec})$ obtained at the same stress level, for temperatures greater than 40°C. It is noteworthy that this deviation of about 5% from linearity occurred at a tensile strain as low as 0.0005. It seems that viscoelastic measurements made on drawn LPE above room temperature, even after extensive annealing, should always be checked especially carefully for reproducibility and linearity of viscoelastic behaviour.

4. Comparison of theory and experiment

4.1. Anisotropy of relaxation due to a simple shear process

This section considers the anisotropy of relaxation magnitude predicted for the present samples by theories I, IIA and IIB, taken in turn. The common feature of these theories, as noted above, is that they assign mechanical relaxation to deformation by simple shear. We begin by simply invoking this property of the theories.

A specimen of LPE is assumed to be composed entirely of many identical structural units, where each unit is a multilayer sandwich of crystalline lamellae (each of thickness about 300 Å) separated by layers (of thickness about 50 Å) containing molecular segments in non-crystalline conformation. Consider each structural unit to contain a set of planes, which we label S-planes, whose normals are parallel to unit vector **N**, such that relaxation occurs when shear stresses act on these planes and parallel to a direction given by unit vector **T**.

During a dynamic tensile test the external tensile stress, of amplitude σ, is applied in the direction of unit vector **F**. Now let the i-th structural unit be oriented such that **F** makes angles $\gamma^{(i)}$ and $\lambda^{(i)}$ with **N** and **T** respectively (see Fig. 11). Assume that all S-planes are subject to a stress system identical to that applied externally to the sample. Then the amplitude of resolved shear stress $\tau_{\mathbf{NT}}{}^{(i)}$ acting on the i-th set of S-planes and parallel to **T** is given by

$$\tau_{\mathbf{NT}}{}^{(i)} = \sigma \cos\gamma^{(i)} \cos\lambda^{(i)} \ . \qquad (6)$$

Now let J'' be the shear loss compliance of the structural unit for shear on S-planes parallel to **T**, and D'' the measured tensile loss compliance of the specimen. Since all structural units are assumed identical they all have identical values of J''. Equating the viscoelastic energy loss per unit volume of specimen per cycle to the energy dissipated on S-planes per cycle then gives

$$D''\,\sigma^2 = J''\,\overline{\tau_{\mathbf{NT}}{}^2} \qquad (7)$$

where a bar placed above denotes the volume average quantity. Combining Equations 6 and 7 yields

$$D'' = J''\,\overline{\cos^2\gamma \cos^2\lambda} \ . \qquad (8)$$

The anisotropy of D'' arises solely from anisotropy of the term $\overline{\cos^2\gamma \cos^2\lambda}$, which is labelled I_θ. Thus Equation 8 may be applied in the form

$$D_\theta'' = J''\,I_\theta \qquad (9)$$

where J'' is a constant for a given oriented sheet of LPE.

All that remains is to evaluate the function I_θ for each theory in turn, when applied to a given oriented sample. Davies *et al* [6] recently performed this calculation for the case where S-planes are lamellar surfaces (i.e., theory I) and the oriented sample has uniaxial symmetry about the draw direction. In the following, this treatment is extended by considering all three theories, I, IIA and IIB and applying them to the two types of biaxially oriented LPE studied here.

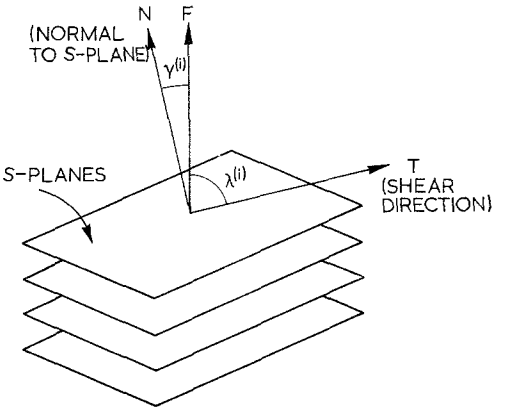

Figure 11 Orientation of i-th set of S-planes with respect to direction **F** of applied tensile stress σ, during a uniaxial tensile test of oriented LPE.

4.2. Application to specific theories

4.2.1. Theory I: interlamellar shear

This theory proposes that S-planes are the surfaces of the lamellar crystals. Within a given

structural unit, therefore, **N** is identified with $\mathbf{n}_l$, unit normal to the lamellae. Now, because of difficulties with the interpretation of small-angle X-ray scattering patterns (see below), $\mathbf{n}_l$ is assumed to have the simple doublet or single orientations shown in the idealized structural models of Fig. 4a and b. In general, therefore, for biaxially oriented LPE, all $\mathbf{n}_l$ are taken to be oriented in the XZ plane at angles $\pm\Omega$ to Z. For present purposes, assume the structural unit to have approximately transverse isotropy about $\mathbf{n}_l$. Then the shear direction **T** will be co-planar with $\mathbf{n}_l$ and **F**, giving $\lambda = 90° - \gamma$ and hence

$$\cos\lambda = \sin\gamma \ . \tag{10}$$

These assumptions are summarized in Fig. 12a. From this diagram, γ is given by

$$\cos\gamma = \mathbf{F} \,.\, \mathbf{n}_l = \cos\theta\cos\Omega \tag{11}$$

and so, making use of Equation 10

$$I_\theta = \cos^2\theta\cos^2\Omega\,[1 - \cos^2\theta\cos^2\Omega] \ . \tag{12}$$

The function I_θ from Equation 12 is shown in Fig. 13a and b for biaxially cold-drawn LPE ($\Omega = 38°$) and biaxially hot-drawn LPE ($\Omega = 0°$) respectively.

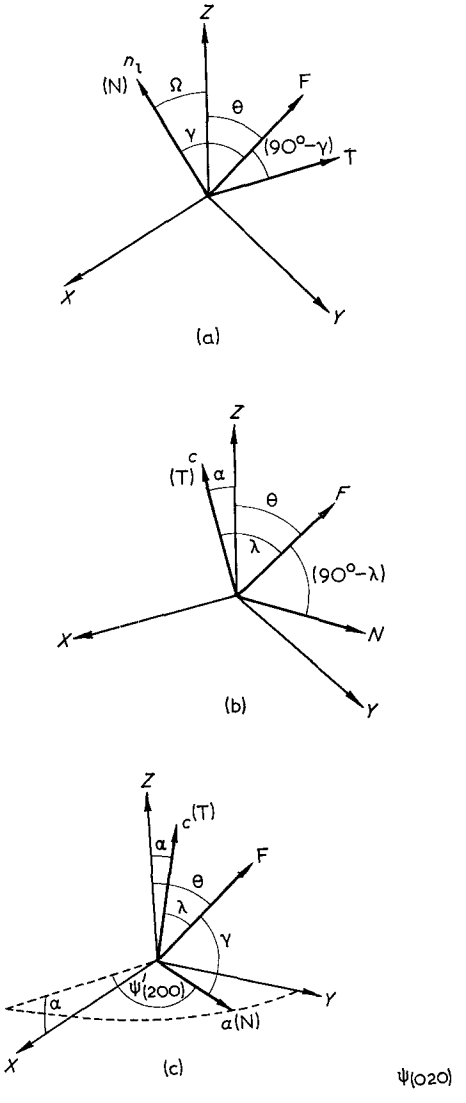

Figure 12 Application to biaxially oriented LPE of: (a) theory I, (b) theory IIA, (c) theory IIB.

4.2.2. Theory IIA: intracrystalline shear

The characteristic feature of both theories IIA and IIB is that the shear direction **T** coincides with crystal c-axes. In each sample of LPE studied here c-axes were highly oriented in the XZ plane in general at an angle of $\pm\alpha$ to Z (see Figs. 2c and 5c). The distributions about these positions will be neglected here.

Theory IIA proposes that relaxation can occur equally in response to shear stresses on all crystal planes of type $(hk0)$. In the present case, assume structural units to have transverse isotropy about c-axes; then shear deformation parallel to **c** will occur on those $(hk0)$ planes whose normals are co-planar with **c** and **F**. S-planes therefore have **N** co-planar with **c** and **F**, and hence $\gamma = 90° - \lambda$, and

$$\cos\gamma = \sin\lambda \ . \tag{13}$$

These assumptions are summarized in Fig. 12b.

Proceeding in a similar manner as before λ is given by

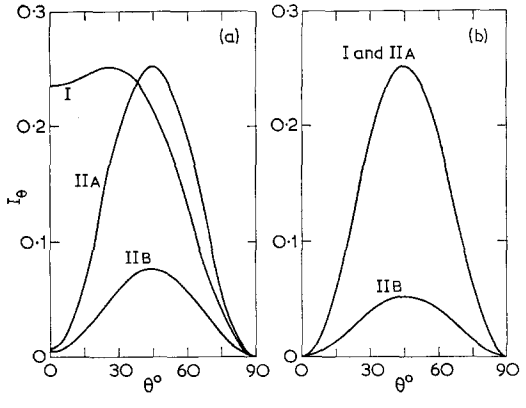

Figure 13 Anisotropy of the α-relaxation in the YZ plane as predicted by theories I, IIA and IIB, for (a) biaxially cold-drawn LPE, (b) biaxially hot-drawn LPE.

$$\cos\lambda = \frac{\mathbf{F}\,.\,\mathbf{c}}{|\mathbf{c}|} = \cos\theta\cos\alpha \qquad (14)$$

and, making use of Equation 13,

$$I_\theta = \cos^2\theta\cos^2\alpha\,[1 - \cos^2\theta\cos^2\alpha]\ . \qquad (15)$$

This function is included in Fig. 13 a and b for biaxially cold-drawn LPE ($\alpha = 5°$) and biaxially hot-drawn LPE ($\alpha = 0°$) respectively.

4.2.3. Theory IIB: intracrystalline shear

This theory is more specific than IIA, since relaxation is confined to shear on (h00) planes. Thus, in addition to the condition that **T** is parallel to **c**, **N** must be parallel to **a** (that is, parallel to the (200) plane normal). This situation is represented in Fig. 12c, again taking c-axes to have simple doublet orientation in the XZ plane at angles $\pm\alpha$ to Z (only the case of $-\alpha$ is shown). All a- and b-axes are therefore confined to planes containing the Y-axis and making angles of $\pm\alpha$ with X. Within these planes let the orientation of a-axes be defined by the angle $\psi'_{(200)}$ shown in Fig. 12c. Similarly let the orientation of b-axes be defined by an angle $\psi'_{(020)}$.

Equation 14 applies in the present case also. Now, however, γ is given by

$$\cos\gamma = \frac{\mathbf{F}\,.\,\mathbf{a}}{|\mathbf{a}|} = \sin\theta\sin\psi'_{(200)} - \cos\theta\sin\alpha\cos\psi'_{(200)} \qquad (16a)$$

or

$$\cos\gamma = \frac{\mathbf{F}\,.\,\mathbf{a}}{|\mathbf{a}|} = \sin\theta\sin\psi'_{(200)} + \cos\theta\sin\alpha\cos\psi'_{(200)} \qquad (16b)$$

depending on whether c-axes are inclined within the XZ plane at $+\alpha$ or $-\alpha$ to Z respectively. Forming the function I_θ, making use of Equations 14, 16a and 16b, then yields

$$I_\theta = \cos^2\theta\cos^2\alpha\,[\sin^2\theta(1 - \overline{\cos^2\psi'_{(200)}}) + \cos^2\theta\sin^2\alpha\,\overline{\cos^2\psi'_{(200)}}]\ . \qquad (17)$$

The averages $\overline{\cos^2\psi'_{(200)}}$ were obtained from pole figures for (020) poles (Figs. 2b and 5b), in order to avoid the effect of some overlap from adjacent (110) poles in (200) pole figures (see Fig. 2a). Since a- and b-axes are orthogonal within each crystal $\overline{\cos^2\psi'_{(200)}} = \overline{\sin^2\psi'_{(020)}}$. Figs. 2b and 5b gave values for $\overline{\cos^2\psi'_{(200)}}$ of 0.702 and 0.793 for biaxially cold-drawn LPE and biaxially hot-drawn LPE respectively. Making use of these values the function I_θ from Equation 17 was evaluated and is included in Fig. 14a and b, again taking $\alpha = 5°$ and $\alpha = 0°$ respectively.

4.3. Comparison with experiment

To compare the above theories with experiment, via Equation 9, the function $D_\theta''(= D_\theta' \tan\delta_\theta)$ is required. This was evaluated from tensile creep data by combining the approximation [18]

$$D'(\omega) \simeq [D(t)]_{\omega=1/t} \qquad (18)$$

with $\tan\delta(\omega)$ obtained from Equation 1. In this way, D_θ'' was calculated for a frequency $\omega = 0.1$ rad sec^{-1} and temperature $T = 20°$C, at $\theta = 0°$, 45° and 90°. These values of D_θ'' and those of D_θ' and $\tan\delta_\theta$ used in their calculation are collected in Table I. The complete θ dependence of D_θ'', for $\omega = 0.1$ rad sec^{-1} and $T = 20°$C, was obtained from D_0'', D_{45}'' and D_{90}'' by applying Equation 4 to D_θ*. The functions D_θ'' obtained from experiment in this way are plotted in Figs. 14a and b for biaxially cold-drawn and biaxially hot-drawn LPE respectively.

TABLE I Values of D_θ' and $\tan\delta_\theta$ (and hence D_θ'') derived from tensile creep data for a radial frequency $\omega = 0.1$ rad sec^{-1} and temperature $T = 20°$C (units of tensile compliance are 10^{-11} cm^2 dyn^{-1}).

Specimen	$\theta°$	D_θ'	$\tan\delta_\theta$	D_θ''
Biaxially cold-drawn LPE	0	5.10	0.191	0.972
	45	7.60	0.128	0.974
	90	4.47	0.054	0.241
Biaxially hot-drawn LPE	0	1.57	0.142	0.222
	45	4.63	0.095	0.439
	90	3.64	0.039	0.143

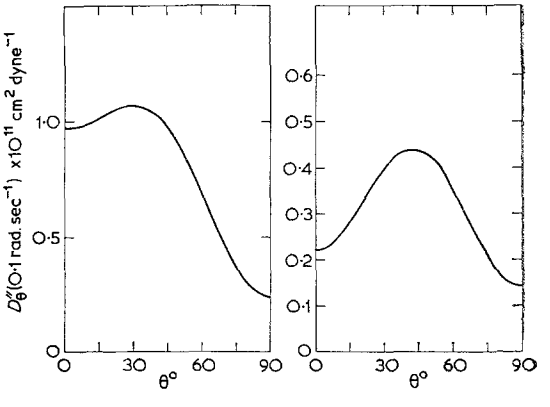

Figure 14 Anisotropy of tensile loss compliance D_θ'' (0.1 rad sec^{-1}), deduced from tensile creep data at a temperature $T = 20°$C, for (a) biaxially cold-drawn LPE, (b) biaxially hot-drawn LPE.

Theory and experiment are compared by simply comparing Fig. 13a with Fig. 14a, and Fig. 13b with Fig. 14b, since D_θ'' should be proportional to I_θ from Equation 9. The result is astonishingly clear. Theory I correctly predicts the anisotropy of D_θ'' for *both* oriented sheets of LPE. On the other hand, theories IIA and IIB are consistent with experiment for biaxially hot-drawn LPE, but are in serious error for biaxially cold-drawn LPE. This clear result gives strong support to the theory of relaxation by an interlamellar shear mechanism. It is, therefore, in accord with the recent conclusions of Davies *et al* [6], derived from measurements made on uniaxially cold-drawn and annealed LPE.

The importance of adopting specific models of the relaxation in order to reach this conclusion must, however, be recognized. Earlier work of Ward and co-workers [5] made the empirical assumption that anisotropy of tan δ is characteristic of the anisotropy of relaxation. The same treatment applied to the present results leads to a conclusion opposite to that reached above, since anisotropy of tan δ was found to be independent of lamellar orientation (compare Figs. 8 and 10). This contradiction probably arises because of the spread of lamellar orientation present in actual samples of oriented LPE. Thus, although theory I predicts $D_{90}'' = 0$ for biaxially cold-drawn LPE (see Fig. 13a) and $D_0'' = D_{90}'' = 0$ for biaxially hot-drawn LPE (see Fig. 13b), the experimental values are in fact finite (see Fig. 14a and b). This can be easily explained on the basis of some spread of $\mathbf{n}_1$ about their mean orientation. Unfortunately, it is not possible to allow for this effect by measuring the distribution of $\mathbf{n}_1$ from broadening of the small-angle X-ray scattering pattern. Broadening from this cause cannot be adequately separated from that due to finite crystal size and paracrystalline distortions [26], and finite X-ray beam diameter.

5. Discussion

5.1. Significance for undrawn LPE

If the mechanical α-relaxation in annealed drawn LPE occurs by simple shear deformation of interlamellar layers, the question immediately follows: what is the significance of this result for undrawn LPE, on which previous measurements have mostly been made?

It is now well established that the microstructure of as-drawn LPE differs markedly from that of undrawn LPE. The drawing process has three drastic effects, in addition to introducing preferred lamellar and crystallographic orientations.

1. Spherulites containing wide lamellar crystals are destroyed, to produce fibres consisting of stacks of smaller crystals. [27-29].
2. Non-crystalline regions suffer molecular alignment and an increase in density [30-33].
3. Crystalline regions are disrupted by the introduction of crystal defects and therefore decrease in density [31, 33].

Undoubtedly, the situation is further complicated by residual stresses which remain after drawing. The mechanical relaxation behaviour of LPE in this form, already studied by several authors [5, 21, 22, 34-38], must be interpreted in the light of such complicating factors, and will not be considered here.

When the drawn polymer is annealed, however, especially above about 120°C, there is a remarkable recovery of the microstructure. Both crystalline and non-crystalline fractions become indistinguishable from their counterparts in undrawn LPE, as detected by a variety of techniques [31, 39-42]. Concurrently, adjacent fibres fuse together to give greater lateral continuity to the lamellar crystals, as observed by electron microscopy [43] and small-angle X-ray scattering [27]. The microstructure of drawn and well-annealed LPE may therefore be assumed identical to that of isotropic spherulitic LPE, except of course for the presence of preferred lamellar and crystallographic orientation. For this reason, the mechanical α-relaxation observed in such oriented specimens may reasonably be identified with the α-relaxation observed at the same temperature (and frequency) in undrawn LPE, crystallized either from the melt or from dilute solution.

5.2. Comparison with dielectric and NMR α-relaxations

Now at a similar temperature/frequency position, LPE exhibits a dielectric relaxation (when lightly oxidized) and narrowing of the wide-line NMR spectrum. There is much evidence that the molecular relaxation observed by these two techniques occurs within the body of crystals [44], probably by means of hindered chain rotation of 180° [8, 45, 46] accompanied by longitudinal displacement of $[00\frac{1}{2}]$ [8, 46]. Furthermore, the mechanical α-relaxation in polyethylene is known to depend for its existence on the presence of polyethylene crystals [47]. How may the present conclusions, assigning mechanical relaxation to

deformation of *non*-crystalline layers, be rationalized in the light of these facts?

Hoffman *et al* [8] suggested that relaxation within the crystals by chain rotation of 180° and longitudinal displacement of $[00\frac{1}{2}]$ would be coupled to the fold-containing crystal surface layers when folds were sufficiently tight (containing the minimum of 5 CH_2 units). Their particular model of the fold surface has been seriously challenged by recent experiments, which suggest more mobile folds [48], but the essence of their argument probably remains valid. Mechanical relaxation could occur as follows in an isochronal experiment. At low temperatures, a sequence of CH_2 units in non-crystalline configuration is effectively pinned at the point (for a cilium) or points (for a chain fold) where it enters the crystal. These points locally restrict the otherwise large-scale motion of the sequence, for temperatures above the γ-relaxation (which has some of the characteristics of a glass-rubber transition [49, 50]. At high temperatures, however, when relaxation of crystalline molecules by chain rotation can occur rapidly, these points become effectively free and release their constraint. By this means, relaxation within the crystal (the dielectric and NMR α-relaxation) could increase the compliance of the non-crystalline surface layers and give rise to mechanical relaxation.

The essential feature of the above suggestion is that the two α-relaxations, observed by dielectric and NMR techniques on the one hand, and by mechanical tests on the other, are coupled but have different molecular origins. Independent evidence that these two relaxations are not identical is obtained by comparing their temperature/frequency positions. Mechanical and dielectric results in the α-region have been compared by Reddish and Barrie [51] and Sandiford and Willbourn [52]. The two techniques yield approximately equal activation energies [52]. Nevertheless, the mechanical α-relaxation lies consistently at higher temperatures (lower frequencies) than the dielectric α-relaxation [51, 52]. Furthermore, McCall and Douglass [53] found the temperature/frequency position of the NMR α-relaxation to agree well with its dielectric counterpart, but to lie at considerably lower temperatures (higher frequencies) than the mechanical α-relaxation.

5.3. Other evidence

From the large body of experimental evidence concerning the α-relaxation in LPE, two items especially lend support to the present model. Firstly, when single crystals of LPE are annealed, the mechanical α-relaxation magnitude increases linearly with reciprocal long period, L^{-1} [54, 55]. This suggests that mechanical relaxation originates within crystal surface folds, whose concentration (neglecting the effect of chain ends) is proportional to L^{-1} [54]. Secondly, high energy irradiation (electrons or γ-rays) of LPE causes crosslinks to be formed in the lamellar surfaces or between lamellae [56]. When LPE is treated in this way the mechanical α-relaxation decreases in magnitude [3, 36, 54, 57]. Clearly, this is further evidence that relaxation occurs within interlamellar regions.

The main challenge to the present conclusions comes from a few observations suggesting that a contribution to the mechanical α-relaxation arises within the crystals. Of these, the most convincing are the finite relaxation magnitude predicted for annealed single crystals when the extrapolation is made $L^{-1} \rightarrow 0$ [54, 55] and the apparent occurrence of the relaxation in extended chain crystals of LPE [36, 58]. Probably, therefore, the crystals themselves do in fact make a contribution because of the concurrent crystal relaxation, observed by dielectric and NMR techniques and acknowledged in the model described above. Nevertheless, the present results suggest that the mechanical α-relaxation in LPE as normally prepared is dominated by the contribution from non-crystalline regions.

It should be noted, however, that in reaching this conclusion theory III (see Introduction), which also assigns mechanical relaxation to the crystals, has been neglected. This theory does not have the special feature of attributing mechanical relaxation to a simple shear deformation, and therefore cannot be examined by the treatment used here. The present work can shed no light on its validity, although it was recently seriously challenged by careful measurements of the anisotropy of narrowing of the wide-line NMR spectrum in the α-region of temperature [46].

6. Conclusions

Anisotropy of the mechanical α-relaxation in biaxially oriented LPE agrees with the predictions of relaxation occurring by interlamellar shear – in accord with uniaxially oriented LPE [6]. It does not agree consistently with relaxation occurring by intracrystalline shear of type $(hk0)$ $[00l]$.

Acknowledgements

The authors are grateful to Dr R. W. Gray for determining the pole figures. Financial support was provided by the Science Research Council.

References

1. S. IWAYANAGI, *Reports Prog. Polymer Phys. Japan* **5** (1962) 135.
2. S. IWAYANAGI and H. NAKANE, *ibid* **7** (1964) 179.
3. N. G. MCCRUM and E. L. MORRIS, *Proc. Roy. Soc.* **A292** (1966) 506.
4. C. NAKAFUKU, K. MINATO, and T. TAKEMURA, *Japan J. Appl. Phys.* **7** (1968) 1155.
5. Z. H. STACHURSKI and I. M. WARD, *J. Macromol. Sci.-Phys.* **B3** (1969) 445.
6. G. R. DAVIES, A. J. OWEN, I. M. WARD, and V. B. GUPTA, *ibid* **B6** (1972) 215.
7. M. TAKAYANAGI, T. ARAMAKI, M. YOSHINO, and K. HOASHI, *J. Polymer Sci.* **46** (1960) 531.
8. J. D. HOFFMAN, G. WILLIAMS, and E. PASSAGLIA, *ibid* **C14** (1966) 173.
9. W. PECHHOLD and S. BLASENBREY, *Kolloid-Z.u.Z. Polymere* **241** (1970) 955.
10. K. TSUGE, H. ENJOJI, H. TERADA, Y. OZAWA, and Y. WADA, *Japan J. Appl. Phys.* **1** (1962) 270.
11. K. TSUGE, *ibid* **3** (1964) 588.
12. K. OKANO, *J. Polymer Sci. C* **15** (1966) 95.
13. R. HAYAKAWA and Y. WADA, *Reports Progr. Polymer Phys. Japan* **11** (1968) 215.
14. T. SETO and T. HARA, *ibid* **9** (1966) 207.
15. C. P. BUCKLEY, R. W. GRAY, and N. G. MCCRUM, *J. Polymer Sci. B* **8** (1970) 341.
16. K. ISHIKAWA, K. MIYASAKA, and M. MAEDA, *ibid A-2* **7** (1969) 2029.
17. J. W. COOPER and N. G. MCCRUM, *J. Mater. Sci.* **8** (1973), to be published.
18. C. ZENER, "Elasticity and Anelasticity of Metals" (University of Chicago Press, 1948).
19. M. A. BIOT, *J. Appl. Phys.* **25** (1954) 1385.
20. R. F. S. HEARMON, "An Introduction to Applied Anisotropic Elasticity" (Oxford University Press, 1961).
21. C. P. BUCKLEY and N. G. MCCRUM, *J. Polymer Sci. A-2* **9** (1971) 369.
22. M. TAKAYANAGI, K. IMADA, and T. KAJIYAMA, *ibid C* **15** (1966) 263.
23. K. OKA and T. KAWAGUCHI, *Reports. Prog. Polymer Phys. Japan* **9** (1966) 385.
24. V. B. GUPTA and I. M. WARD, *J. Macromol. Sci-Phys. B* **2** (1968) 89.
25. H. GODDAR, G. F. SCHMIDT, and E. W. FISCHER, *Makromol. Chem.* **127** (1969) 286.
26. R. HOSEMANN, *J. Polymer Sci. C* **20** (1967) 1.
27. R. BONART and R. HOSEMANN, *Kolloid-Z.u.Z. Polymere* **186** (1962) 16.
28. A. PETERLIN and K. SAKAOKU, *ibid* **212** (1966) 51.
29. W. GLENZ, A. PETERLIN, and W. WILKE, *J. Polymer Sci. A-2* **9** (1971) 1243.
30. R. S. STEIN and B. E. READ. *Appl. Polymer Symp.* **8** (1969) 255.
31. E. W. FISCHER, H. GODDAR, and G. F. SCHMIDT, *J. Polymer Sci. A-2* **7** (1969) 37.
32. W. GLENZ and A. PETERLIN, *ibid A-2* **9** (1971) 1191.
33. W. GLENZ, N. MOROSOFF, and A. PETERLIN, *ibid B* **9** (1971) 211.
34. K. H. HELLWEGE, R. KAISER, and K. KUPHAL, *Kolloid-Z.* **157** (1958) 27.
35. Z. H. STACHURSKI and I. M. WARD, *J. Polymer Sci. A-2* **6** (1968) 1083.
36. K. H. ILLERS, *Kolloid-Z.u.Z. Polymere* **231** (1969) 622.
37. K. A. WOLF, *ibid* **231** (1969) 656.
38. E. W. FISCHER, H. GODDAR, and W. PIESCZEK, *J. Polymer Sci. C* **32** (1971) 149.
39. A. PETERLIN and H. G. OLF, *ibid A-2* **4** (1966) 587.
40. G. MEINEL and A. PETERLIN, *ibid B* **5** (1967) 613.
41. A. PETERLIN, J. L. WILLIAMS, and V. STANNETT, *ibid A-2* **5** (1967) 957.
42. I. M. WARD and T. WILLIAMS, *J. Macromol. Sci.-Phys. B* **5** (1971) 693.
43. A. PETERLIN and K. SAKAOKU, *J. Appl. Phys.* **38** (1967) 4152.
44. N. G. MCCRUM, B. E. READ, and G. WILLIAMS, "Anelastic and Dielectric Effects in Polymeric Solids" (Wiley, London, 1967).
45. C. A. F. TUIJNMAN, *Polymer* **4** (1963) 315.
46. H. G. OLF and A. PETERLIN, *J. Polymer Sci. A-2* **8** (1970) 771.
47. K. SCHMIEDER and K. A. WOLF, *Kolloid-Z.* **134** (1953) 149.
48. A. PETERLIN, *J. Macromol. Sci.-Phys. B* **3** (1969) 19.
49. E. W. FISCHER and F. KLOOS, *J. Polymer Sci. B* **8** (1970) 685.
50. F. C. STEHLING and L. MANDELKERN, *Macromolecules* **3** (1970) 242.
51. W. REDDISH and J. T. BARRIE, IUPAC Symposium, Weisbaden, 1959, Paper 1A3.
52. D. J. H. SANDIFORD and A. H. WILLBOURN, in "Polythene" 2nd Ed. A. Renfrew and P. Morgan Eds. (Ilife, London, 1960).
53. D. W. MCCALL and D. C. DOUGLASS, *Appl. Phys. Letters* **7** (1965) 12.
54. K. M. SINNOTT, *J. Appl. Phys.* **37** (1966) 3385.
55. M. TAKAYANAGI and T. MATSUO, *J. Macromol. Sci.-Phys. B* **1** (1967) 407.
56. T. KAWAI, A. KELLER, A. CHARLESBY, and M. G. ORMEROD, *Phil. Mag.* **12** (1965) 657.
57. A. W. THORNTON, D.Phil. thesis, Oxford University, 1968.
58. M. TAKAYANAGI, *Pure and Appl. Chemistry* **23** (1970) 151.

Received 21 July 1972 and accepted 1 January 1973.